Electronic Supplementary Material (ESI) for Green Chemistry.

Pd-catalyzed Decarboxylation of Glutamic Acid and Pyroglutamic Acid to Bio-based 2-Pyrrolidone

Free De Schouwer, Laurens Claes, Nathalie Claes, Sara Bals and Dirk E. De Vos*

Supporting Information

1. General

1.1 Chemicals

Pyroglutamic acid (Sigma Aldrich, ≥ 99%), L-glutamic acid (Sigma Aldrich, 99%), 2-pyrrolidone (Sigma Aldrich, ≥ 99%), δ-valerolactam (Sigma Aldrich, 98%), ε-caprolactam (Sigma Aldrich, 99%), γ-aminobutyric acid (Sigma Aldrich, ≥ 99%), propionic acid (Janssen Chimica, 99%), cyclopentanecarboxylic acid (Fluka, 97%), poly(vinyl alcohol) (Sigma Aldrich, average M_W 85 000 - 146 000, 87 - 89% hydrolyzed), $Mg(NO_3)_2.6H_2O$ (Chem-Lab, ≥ 99%), $Al(NO_3)_3.9H_2O$ (Sigma Aldrich, ≥ 98%), $Ba(NO_3)_2$ (Acros, 99%) and $Ca(NO_3)_2.4H_2O$ (Fluka, ≥ 99%) were all used as received. Used catalysts, supports and precursors were Pd/C (5 wt%, Johnson Matthey), $Pd/BaSO_4$ (5 wt%, Johnson Matthey), Pt/C (5 wt%, Johnson Matthey), Al_2O_3 (Condea Chemie, Puralox NGa-150), ZrO_2 (Alfa Aesar), SiO_2 (Aerosil 380), $Pd(NH_3)_4Cl_2.H_2O$ (Sigma Aldrich, ≥ 99.99%), $PdCl_2$ (Sigma Aldrich, 99%) and $Pt(NH_3)_4Cl_2.H_2O$ (Sigma Aldrich, ≥ 99.99%).

1.2 Thermodynamic calculations

Thermodynamic calculations were performed for reactions

$$Pyrrolidone + 3H_2O \rightarrow NH_3 + PA + CO_2 + 2H_2 \tag{2}$$

$$3Pyrrolidone + 5H_2O \rightarrow 3\,PA + NH_3 + CO_2 + 2CH_3NH_2 \tag{4}$$

with Aspen Plus® software. For thermodynamic equilibrium calculations an Equilibrium base reactor, REquil, was used with two output streams (vapor VapEquil and liquid LiqEquil), which were combined into one PRDEquil output stream. The REquil reactor block is an equilibrium reactor for chemical reactions in the presence of a user-supplied reaction stoichiometry. The reaction stoichiometry was inserted as suggested in reaction (2) and (4). In this way Aspen Plus® can calculate equilibrium concentrations following the proposed reaction stoichiometry using thermodynamic data from its database for each component. The feed composition for both reactions was inserted in terms of flow rates: 1 kmol/s 2-pyrrolidone and 250 kmol/s water (because of a very large excess). The thermodynamic 'Property Model' was PSRK (predictive Soave-Redlich-Kwong, typically used for higher pressures), with temperature and pressure varying between 127°C and 277°C and 20-45 bar, respectively. With these parameters the output streams were calculated for 2-pyrrolidone and propionic acid (PA) for reaction (2) (Figure S1) and for 2-pyrrolidone, propionic acid and methylamine for reaction (4) (Figure S2) at different temperatures and pressure. Both graphs show that at working conditions (250 °C and 30-45 bar) the thermodynamic equilibrium of reaction (2) and (4) is completely shifted towards the products. However, it is important to mention that this is a thermodynamic equilibrium and thus no kinetic information was assumed in these calculations.

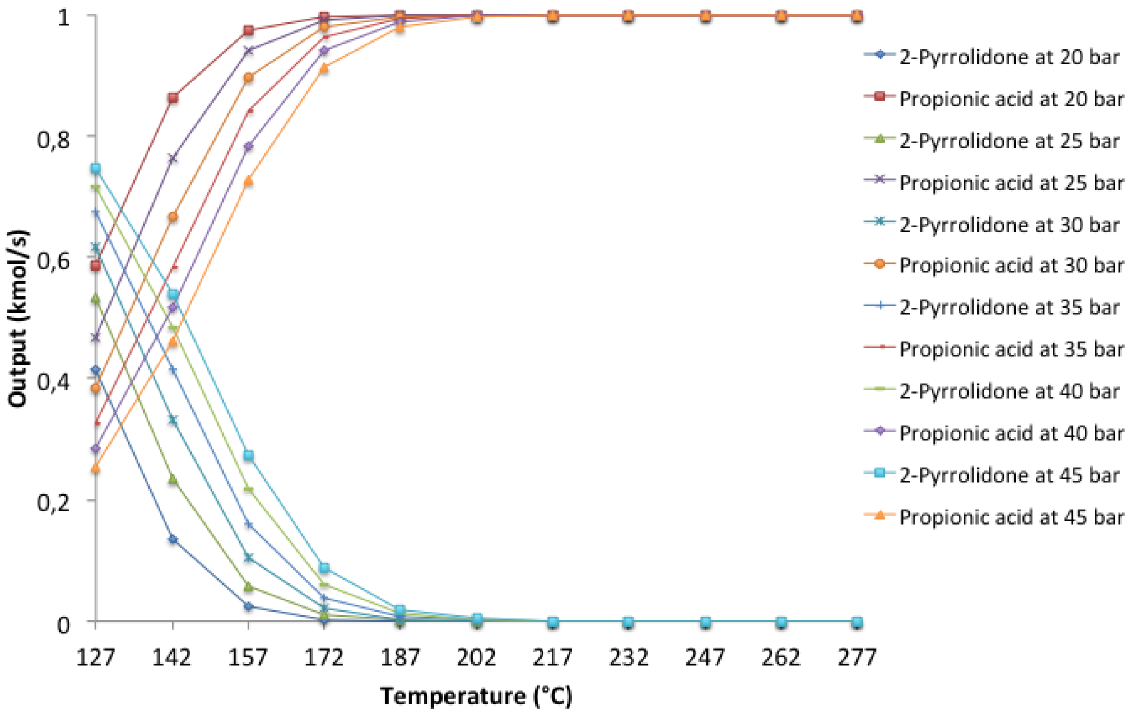

Figure S1. Output stream of 2-pyrrolidone and propionic acid of reaction (2) at 127°C-277°C and 20-45 bar; feed:1 kmol/s 2-pyrrolidone and 250 kmol/s H_2O; reactor REquil; property model PSRK.

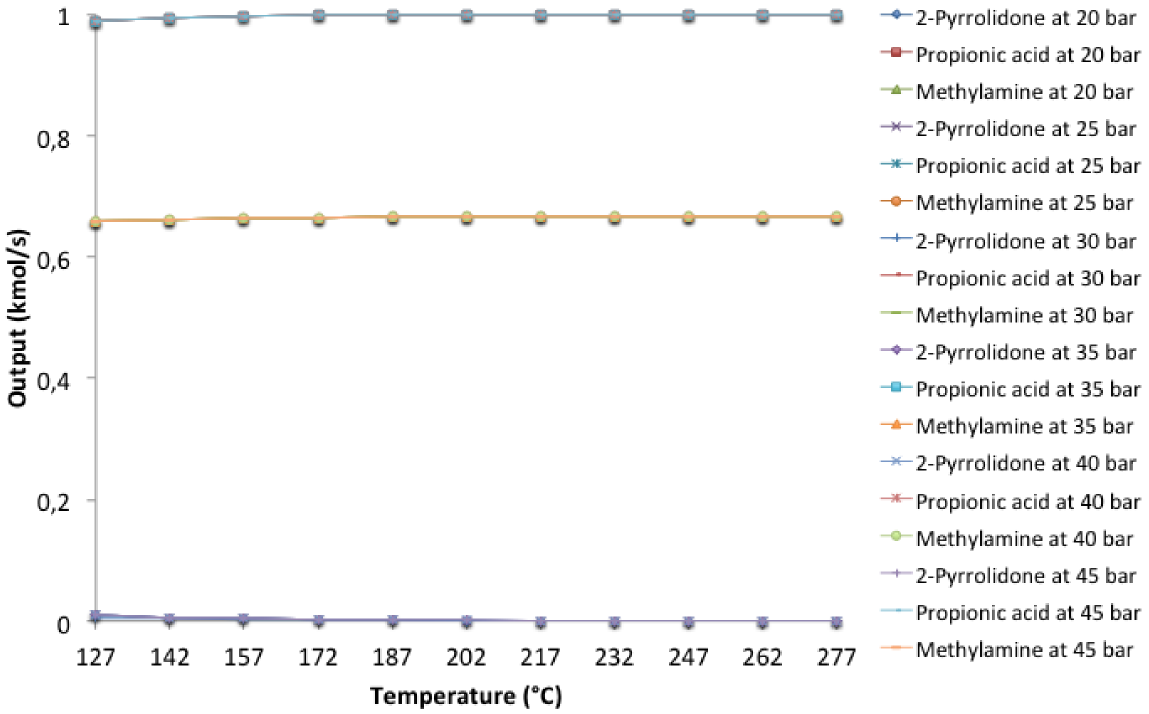

Figure S2. Output stream of 2-pyrrolidone, propionic acid and methylamine of reaction (4) at 127°C-277°C and 20-45 bar; feed:1 kmol/s 2-pyrrolidone and 250 kmol/s H_2O; reactor REquil; property model PSRK.

2. Catalyst characterisation

2.1 Powder X-ray diffraction (XRD)

Powder X-ray diffraction patterns were determined for the synthesized catalysts and their supports (except for the amorphous silica) (Figure S3). After loading the catalysts with palladium, all supports maintain most of their crystallinity. In the case of the Pd/SiO_2 catalyst, clear Pd(0) peaks are present, suggesting that large Pd particles were formed. Additional TEM measurements (Figure S5) demonstrated that Pd particles (7-9 nm) were larger for the Pd/SiO_2 catalyst compared to the other materials. The XRD patterns of the spinel materials correspond to those from literature, indicating a successful synthesis.[S1] However, $BaCO_3$ was present as an additional crystalline phase in the case of $BaAl_2O_4$.

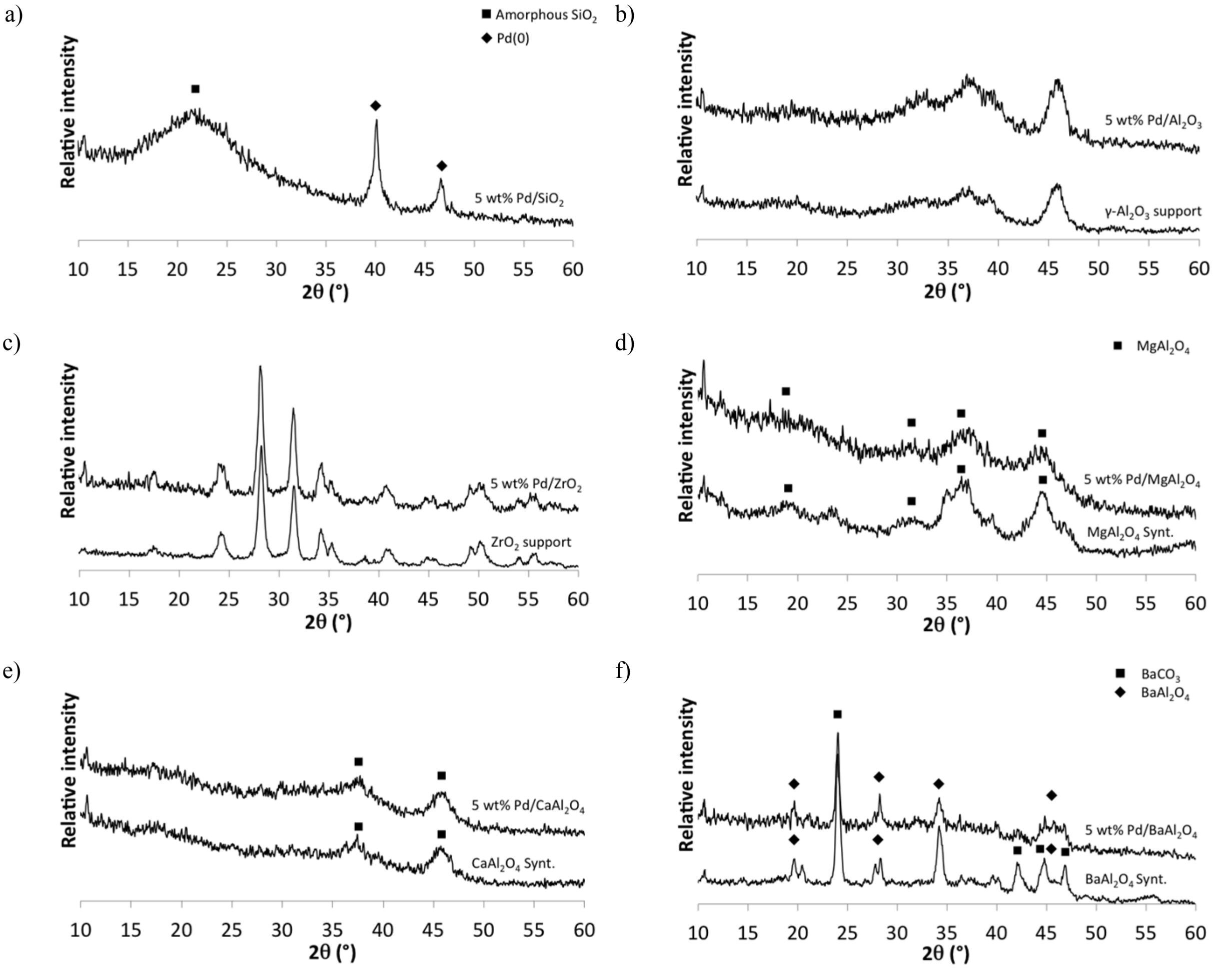

Figure S3. Powder X-ray diffraction patterns of a) 5 wt% Pd/SiO_2, b) commercial Al_2O_3 support and 5 wt% Pd/Al_2O_3, c) commercial ZrO_2 support and 5 wt% Pd/ZrO_2, d) as-synthesized $MgAl_2O_4$ (Synt.) and 5 wt% Pd/$MgAl_2O_4$, e) as-synthesized $CaAl_2O_4$ (Synt.) and 5 wt% Pd/$CaAl_2O_4$ and f) as-synthesized $BaAl_2O_4$ (Synt.) and 5 wt% Pd/$BaAl_2O_4$.

2.2 Nitrogen physisorption

The textural properties of the synthesized palladium catalysts were determined from nitrogen physisorption measurements at 77 K (Figure S4). The adsorption-desorption isotherms of Pd/SiO_2, Pd/Al_2O_3 and Pd/ZrO_2 (a-c) show type IV-behaviour according to the IUPAC classification, which is typical for materials with a limited micropore structure. The isotherms exhibit a hysteresis loop, which is typically associated with a mesoporous structure and originates from the SiO_2, Al_2O_3 and ZrO_2 supports. The high surface area spinel materials (d-f) follow a type II- or a pseudo type II-behaviour: the hysteresis loop of Pd/$MgAl_2O_4$ and Pd/$BaAl_2O_4$ (d and f) is small but typical for slit-shaped pores; the pore volume is, however, rather low. The isotherms of Pd/$CaAl_2O_4$ exhibit almost no hysteresis, implying a non-porous or macroporous material. The surface areas of the spinel materials are high, which was expected according to the synthesis in the presence of poly(vinyl alcohol).

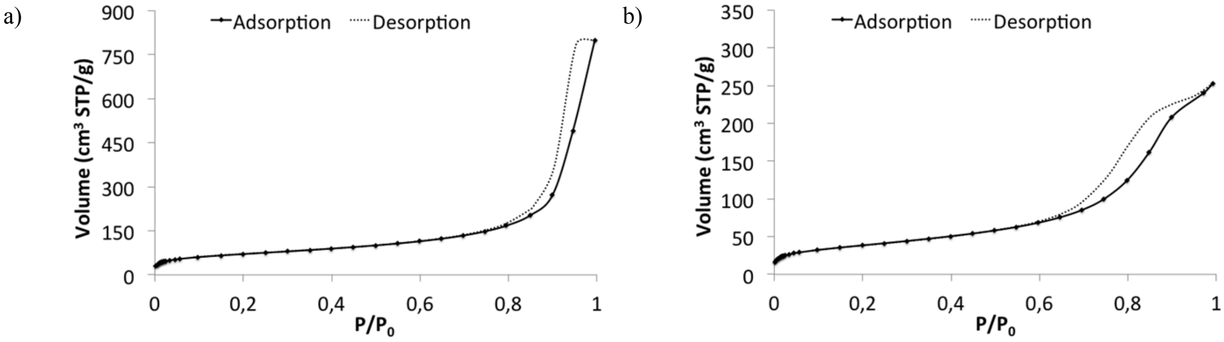

BET surface = 253 m^2/g

BET surface = 138 m^2/g

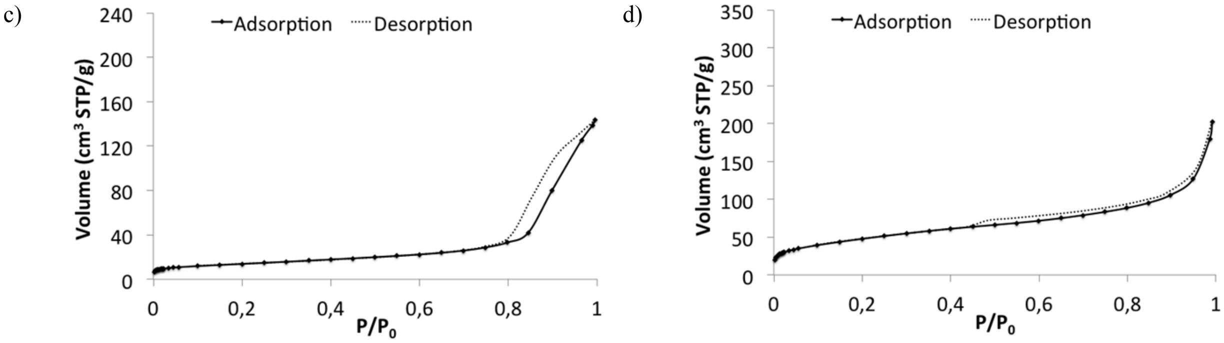

BET surface = 49 m^2/g

BET surface = 175 m^2/g

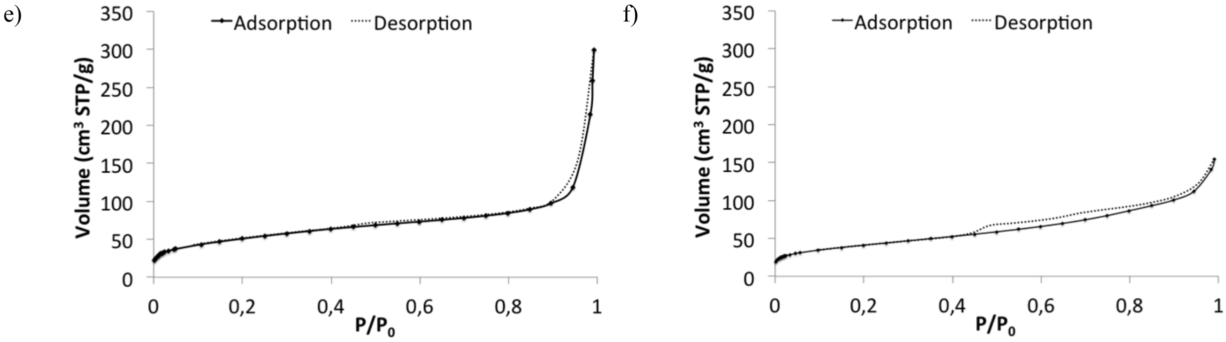

BET surface = 183 m^2/g

BET surface = 146 m^2/g

Figure S4. Nitrogen physisorption isotherms and BET surface area of a) Pd/SiO_2, b) Pd/Al_2O_3, c) Pd/ZrO_2, d) Pd/$MgAl_2O_4$, e) Pd/$CaAl_2O_4$ and Pd/$BaAl_2O_4$.

2.3 High Angle Annular Dark Field Scanning Transmission Electron Microscopy (HAADF-STEM) and Energy Dispersive X-ray Spectroscopy (EDX)

HAADF-STEM measurements were performed on Pd/SiO_2, Pd/$MgAl_2O_4$, Pd/ZrO_2 and Pd/Al_2O_3 catalysts to determine the size distribution of the Pd particles on the support surface. For Pd/SiO_2 the particle size distribution was determined with 240 palladium particles. Figure S5a-b shows that a well-dispersed material was synthesized with rather large palladium particles. The relatively large size of the Pd particles was already suggested by XRD diffractograms, in which the diffraction pattern of Pd(0) was clearly identified. The number average particle diameter of the Pd/SiO_2 equals 8.8 nm. For Pd/$MgAl_2O_4$ the particle size distribution was determined with 350 palladium particles. In contrast to Pd/SiO_2, a large fraction of smaller particles (< 3 nm) is formed on the surface of $MgAl_2O_4$ (Figure S6a-b). However, a broad range of larger particles was present in the material as well, which increases the number average particle diameter to 6.6 nm. For Pd/ZrO_2 the particle size distribution was determined with 150 palladium particles. Because of the high and comparable atomic weight of Zr and Pd it is difficult to distinguish the Pd particles from Zr by contrast. Therefore, extra EDX measurements were performed in combination with HAADF-STEM (Figure S7b). By combining both techniques it was possible to calculate the particle size distribution, as plotted in Figure S7a. In this case, it can be seen that the material contains a very narrow particle size distribution around 3 nm, and a number average particle diameter of 5.6 nm was calculated. Finally, the particle size distribution of Pd/Al_2O_3 was determined with 260 particles. Like for Pd/$MgAl_2O_4$, Pd/Al_2O_3 had a narrow distribution containing a large fraction of small particles (< 2.5 nm) and also a substantial fraction of larger particles, leading to a number average particle diameter of 3.7 nm (Figure S8a-b).

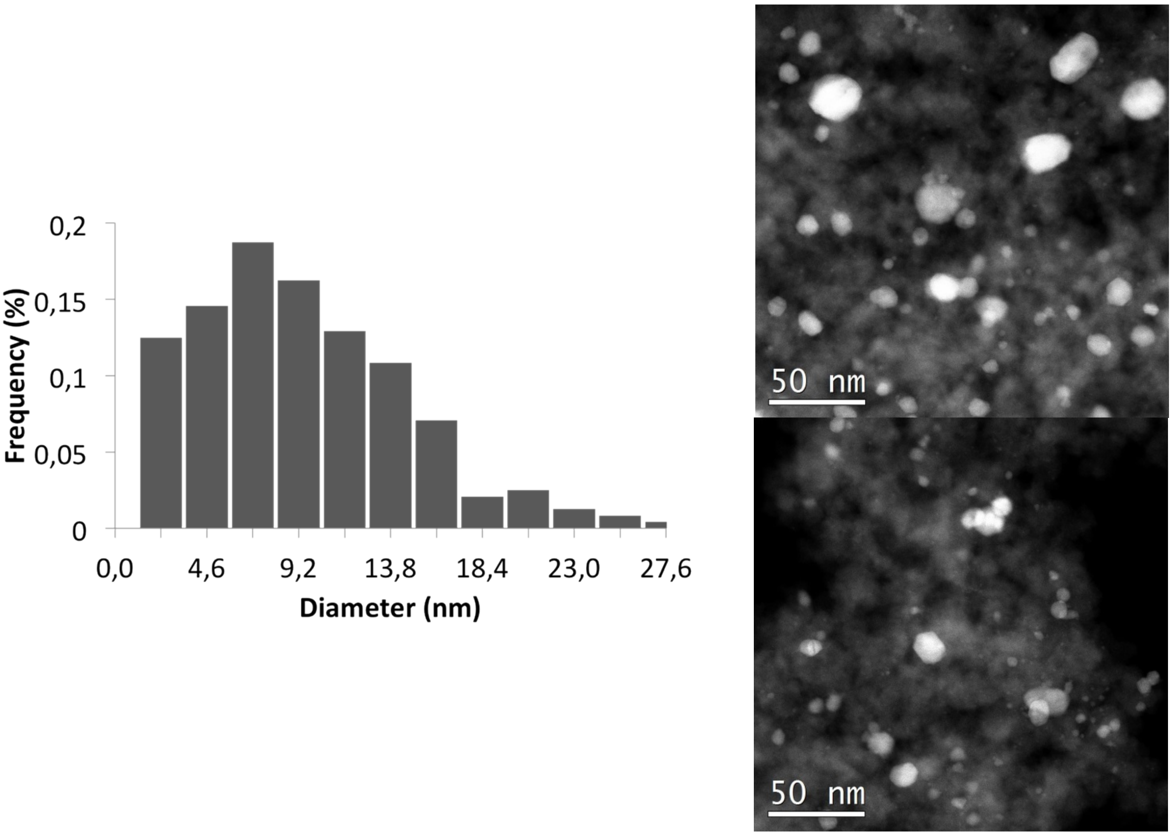

Figure S5. a) Particle size distribution of Pd/SiO_2; b) HAADF-STEM pictures of Pd/SiO_2.

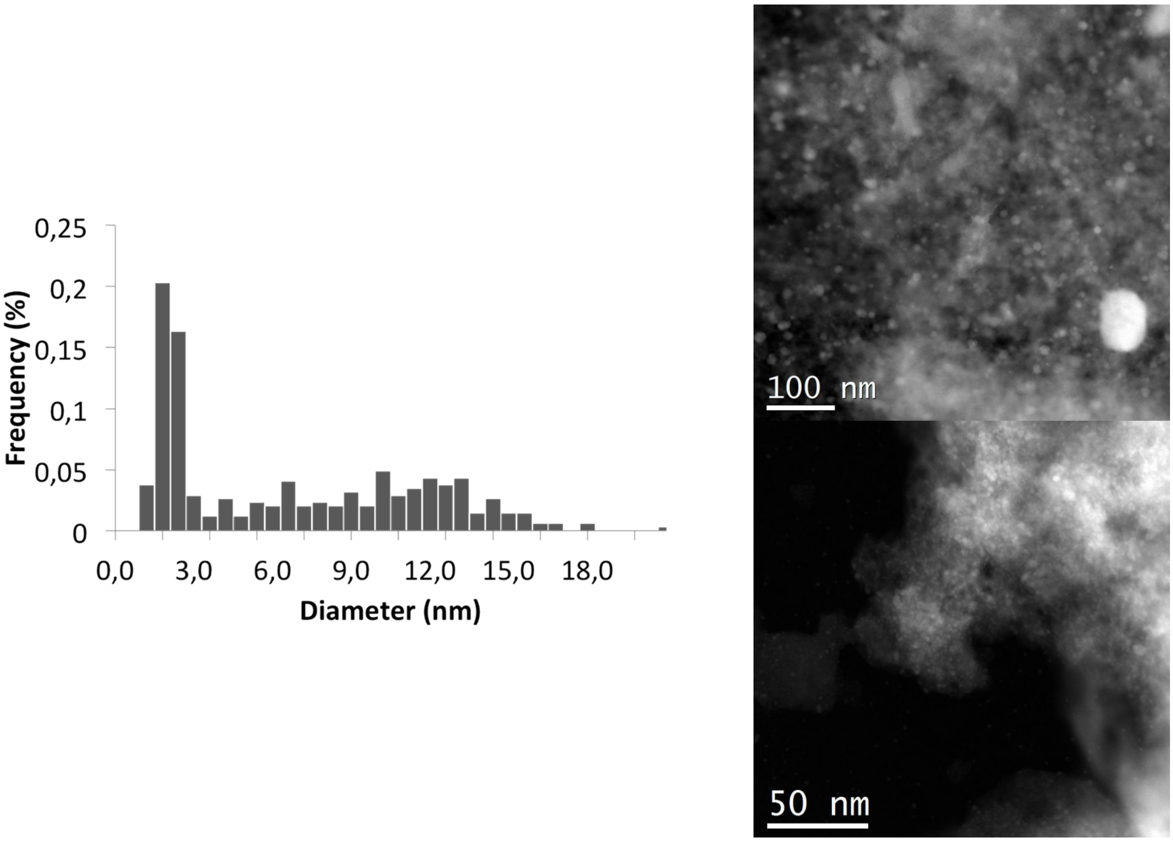

Figure S6. a) Particle size distribution of Pd/$MgAl_2O_4$; b) HAADF-STEM pictures of Pd/$MgAl_2O_4$.

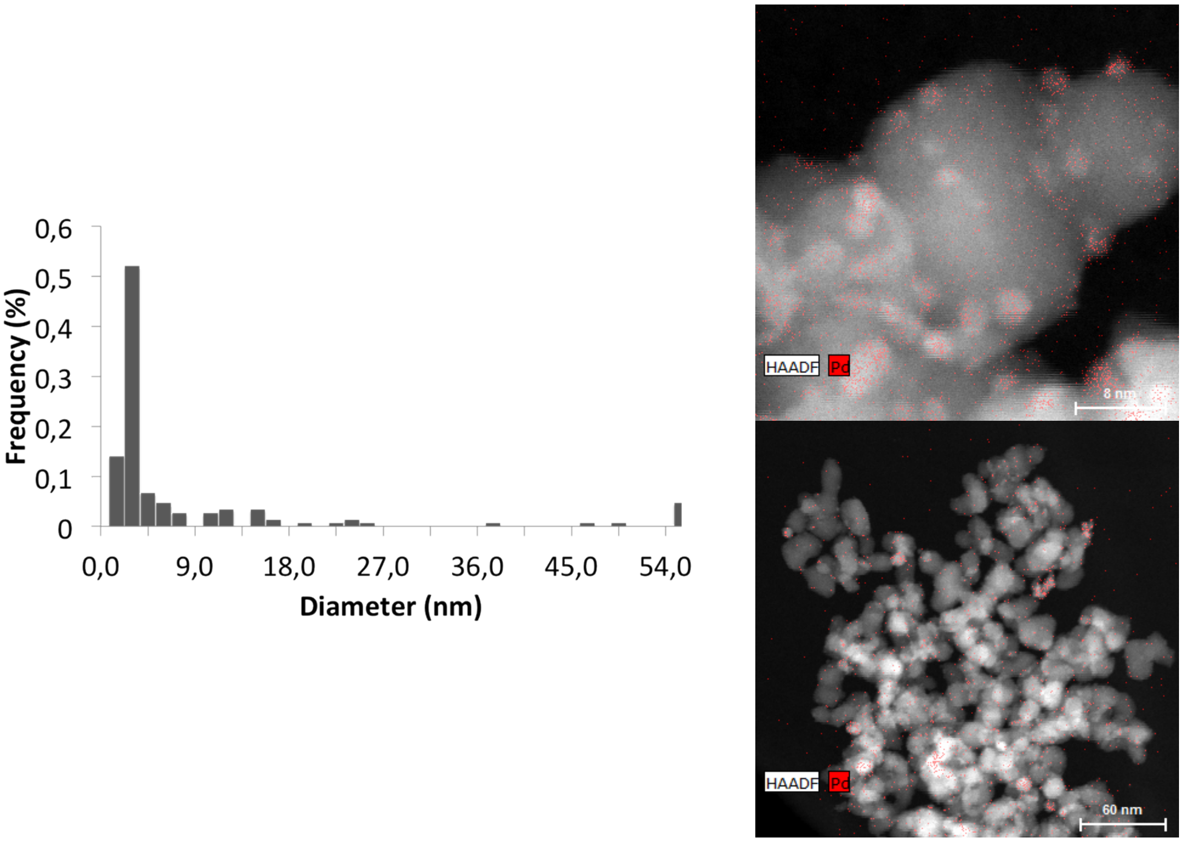

Figure S7. a) Particle size distribution of Pd/ZrO_2; b) HAADF-STEM and EDX pictures of Pd/ZrO_2; the areas with a high probability for Pd are highlighted in red.

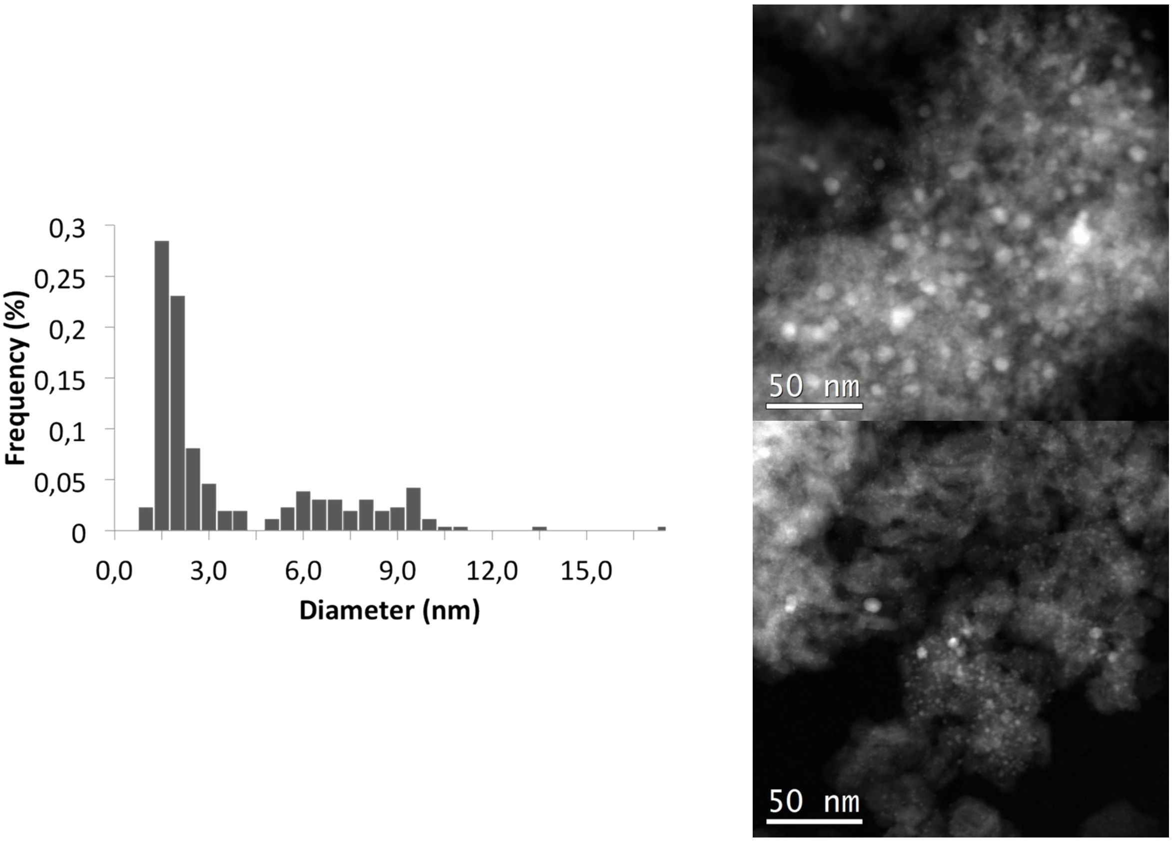

Figure S8. a) Particle size distribution of Pd/Al_2O_3; b) HAADF-STEM pictures of Pd/Al_2O_3.

2.4 Acid-base properties of the catalysts

To distinguish acid-base properties of the different catalysts, the catalysts (50 mg) were suspended in H_2O (3 ml) and stirred for 6 h, after which the pH was measured (Table S1).

Table S1. Acid-base properties of the catalysts.

Catalyst	pH
Pd/C	6.01
Pt/C	5.31
Pd/Al_2O_3	4.53
Pt/Al_2O_3	5.11
Pd/ZrO_2	3.67
Pd/SiO_2	4.46
$Pd/BaSO_4$	6.80
$Pd/CaAl_2O_4$	7.93
$Pd/BaAl_2O_4$	7.81
$Pd/MgAl_2O_4$	8.85

3. Product identification

Pyroglutamic acid (MW = 129 g/mol)

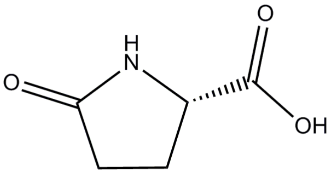

^{1}H-NMR (400 MHz, D_2O): 4.33 - 4.10 ppm (q, ^3J = 4.82 Hz, 1H; -NH-C**H**-COOH), 2.47 ppm (m, 1H; (-NH)(COOH)>CH-HC**H**-), 2.35-2.33 (m, 1H; (-NH)(COOH)>CH-**H**CH-), 2.09 - 2.00 ppm (m, 2H; (-NH-C**H**$_2$-HCH-CH<).

2-Pyrrolidone (MW = 85 g/mol)

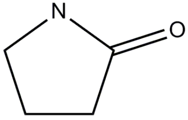

^{1}H-NMR (400 MHz, D_2O): δ = 3.35 ppm (t, ^3J(H,H) = 7.08 Hz, 2H; -CH$_2$-C**H**$_2$-NH-CO-), 2.28 ppm (t, ^3J(H,H) = 8.20 Hz, -CO-C**H**$_2$-CH$_2$-CH$_2$-NH-), 2.06 ppm (quin, ^3J(H,H) = 7.82 Hz, 2H; -CH$_2$-C**H**$_2$-CH$_2$-NH-).
^{13}C-NMR (150.9 MHz, D_2O): 181 ppm (1C, -NH-**C**O-CH$_2$), 41 ppm (1C, -**C**H$_2$-NH-CO), 29 ppm (1C; -NH-CO-**C**H$_2$-), 19 ppm (1C, -**C**H$_2$-CH$_2$-NH-CO-).
^{15}N-NMR (60.8 MHz, D_2O): -258 ppm (1N; CH$_2$-**N**H-CO).
GC/MS (EI, 70 eV): m/z (rel. int., %): 85 (100), 85 (23), 56 (8), 42 (18), 41 (19), 40 (5).

Propionic acid (MW = 74 g/mol)

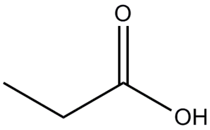

^{1}H-NMR (400 MHz, D_2O): 2,13 - 2,15 ppm (q, ^3J(H,H) = 7.68 Hz, 2H; CH$_3$-C**H**$_2$-COOH), 0,99 ppm (t, ^3J(H,H) = 7,61 Hz, 3H; C**H**$_3$-CH$_2$-COOH).
^{13}C-NMR (150.9 MHz, D_2O): 183 ppm (1C; -CH$_2$-**C**OOH), 29 ppm (1C; CH$_3$-**C**H$_2$-COOH), 9 ppm (1C; **C**H$_3$-CH$_2$-).
GC/MS (EI, 70 eV): m/z (rel. int., %): 74 (100), 73 (63), 57 (29), 56 (16), 55 (18), 45 (32), 44 (5), 42 (6).

γ-Hydroxybutyric acid (GHB) (MW = 104 g/mol)

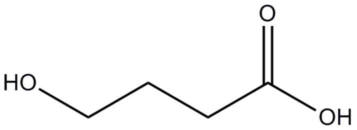

^{1}H-NMR (400 MHz, D_2O): 3.35 ppm (t, ^3J(H,H) = 6.51 Hz, 2H; HO-C**H**$_2$-CH$_2$-), 2.34 ppm (t, ^3J = 7.20 Hz, 2H; -CH$_2$-C**H**$_2$-COOH), 1.73 ppm (quin, ^3J = 7.20 Hz, 2H; -CH$_2$-C**H**$_2$-CH$_2$-).
GC/MS (EI, 70 eV): m/z (rel. int., %): 86 (44), 85 (19), 57 (10), 56 (37), 55 (12), 44 (11), 43 (11), 42 (100), 41 (87), 40 (20), 39 (17).

γ-Butyrolactone (GBL) (MW = 86 g/mol)

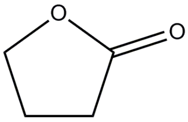

^{1}H-NMR (400 MHz, D$_2$O): 4.38 ppm (t, ^3J = 7.11 Hz, 2H; -CH$_2$-C$\underline{\mathbf{H}}_2$-O-), 2.52 ppm (t, ^3J = 8.15 Hz, 2H; -CH$_2$-C$\underline{\mathbf{H}}_2$-CO-), 2.31 (quin, ^3J = 7.61 Hz, 2H; -CH$_2$-C$\underline{\mathbf{H}}_2$-CH$_2$-)
GC/MS (EI, 70 eV): m/z (rel. int., %): 86 (54), 85 (20), 57 (9), 56 (29), 55 (11), 42 (100), 41 (60), 40 (21), 39 (24), 38 (7).

Methylamine (MW = 31 g/mol)

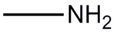

^{1}H-NMR (600 MHz, D$_2$O): 2.36 ppm (3H; C$\underline{\mathbf{H}}_3$-NH$_2$).
^{13}C-NMR (150.9 MHz, D$_2$O): 33 ppm (1C; $\underline{\mathbf{C}}$H$_3$-NH$_2$).
^{15}N-NMR (60.8 MHz, D$_2$O): -361 ppm (1N; CH$_3$-$\underline{\mathbf{N}}$H$_2$).

Butyric acid (MW = 88 g/mol)

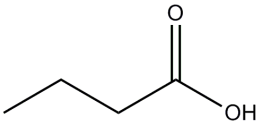

^{1}H-NMR (400 MHz, D$_2$O): 2.10 ppm (t, ^3J(H,H) = 7.41 Hz, 2H; -CH$_2$-C$\underline{\mathbf{H}}_2$-COOH), 1.49 ppm (sex, ^3J(H,H) = 7.41 Hz, 2H; CH$_3$-C$\underline{\mathbf{H}}_2$-CH$_2$-), 0.82 ppm (t, ^3J(H,H) = 7.47 Hz, 3H; C$\underline{\mathbf{H}}_3$-CH$_2$-).
GC/MS (EI, 70 eV): m/z (rel. int., %): 73 (49), 60 (100), 55 (15), 45 (20), 43 (12), 42 (26), 41 (15), 40 (6), 39 (11), 38 (5).

Pentanoic acid (MW = 102 g/mol)

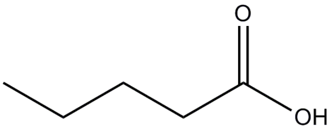

^{1}H-NMR (400 MHz, D$_2$O): 2.11 ppm (t, ^3J(H,H) = 7.42 Hz, 2H; -CH$_2$-C$\underline{\mathbf{H}}_2$-COOH), 1.45 ppm (quin, ^3J(H,H) = 7.37 Hz, 2H; -CH$_2$-C$\underline{\mathbf{H}}_2$-CH$_2$-COOH), 1.22 ppm (sex, ^3J(H,H) = 7.47 Hz, 2H; CH$_3$-C$\underline{\mathbf{H}}_2$-CH$_2$-), 0.81 ppm (t, ^3J = 7.42 Hz, 3H; C$\underline{\mathbf{H}}_3$-CH$_2$-).
GC/MS (EI, 70 eV): m/z (rel. int., %): 87 (5), 74 (5), 73 (48), 61 (6), 60 (100), 55 (14), 43 (9), 42 (11), 41 (15), 39 (12).

Pyrrolidine (MW = 71 g/mol)

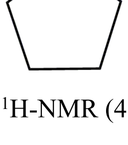

^{1}H-NMR (400 MHz, D$_2$O): 3.21 ppm (t, ^3J(H,H) = 7.10 Hz, 4H; -C$\underline{\mathbf{H}}_2$-NH-C$\underline{\mathbf{H}}_2$-), 1.93 ppm (t, ^3J = 7.25 Hz, 4H; -CH$_2$-C$\underline{\mathbf{H}}_2$-C$\underline{\mathbf{H}}_2$-CH$_2$-).
GC/MS (EI, 70 eV): m/z (rel. int., %): 71 (54), 70 (80), 68 (8), 43 (100), 42 (30), 41 (15), 39 (15).

References

S1 P. G. N. Mertens, S. L. F. Corthals, X. Ye, H. Poelman, P. A. Jacobs, B. F. Sels, I. F. J. Vankelecom and D. E. De Vos, *J. Mol. Catal. A: Chem.*, 2009, **313**, 14-21